

# Vison manipulation with local magnetic fields

Haoran Wang<sup>1,\*</sup> and Alessandro Principi<sup>1,†</sup>

<sup>1</sup>*Department of Physics and Astronomy, University of Manchester, Manchester M13 9PL, UK*

Quantum spin liquids hosting non-abelian anyons have recently experienced renewed interest following the discovery of a variety of materials proximate to these quantum phases. Their anyonic excitations have potential for application to topological quantum computation, but designing logical operations with reduced poisoning requires developing protocols to faithfully create, move and read-out such quasiparticles. In this paper, we present one such protocol for manipulating  $Z_2$  fluxes (“visons”) of ferromagnetic and antiferromagnetic Kitaev models perturbed by a small uniform magnetic field. Our design employs a local driving magnetic field and can achieve high probabilities of generating and displacing flux pairs of both the  $A_z$  and  $B$  phases of the model.

*Introduction*—One of the main challenges to bring about large-scale quantum computation is decoherence [1–5] of quantum states employed. While error-correction codes [6–12] have been designed, they usually require duplication of information over several physical qubits to encode a single logical qubit. This fact hinders scalability of quantum computer architectures. It is thus highly desirable to develop qubits that are by their own design robust against noise.

Topological quantum computation [13–17] offers a potential solution to the decoherence problem. In certain topologically ordered quantum systems, for example in the Kitaev toric code [14], the ground state manifold of the Hilbert space fractures into different independent sectors [18]. In order to go from one sector to another, one must apply a chain of operators whose length scales with the dimensions of the system. It follows that a quantum superposition of states in different sectors is, in a macroscopic system, naturally protected from decoherence. It is in fact unlikely for environmental noise to produce a sufficiently long (and non-local) string of operators that can irreparably damage the quantum state of the system. In this computation scheme, the manipulation of quantum states is achieved by braiding excitations [19] which are, in general, anyons (*i.e.* they behave as neither bosons nor fermions). When one such particle is dragged around another, the state of the system is unitarily rotated in the ground state manifold and a quantum gate is effectively applied on it. Thus, quantum algorithms can be elegantly designed by braiding anyonic excitations.

The Kitaev model [20–24] of a quantum spin liquid, a close relative of the toric code [20], offers a platform for the generation and manipulation of abelian and non-abelian anyons [20, 25]. These have the form of flux-like excitations of the effective gauge field that emerges from the fractionalization of spin variables at each lattice site. Such excitations are conserved in the absence of external magnetic fields. Here, we study the generation of such fluxes (also called vortices or visons) via the application of a local magnetic field in two distinct phases of the Kitaev model. We find that in both of them it is possible to generate and displace vortices with a reasonably high fidelity. Thus, our work paves the way to the development of algorithm to perform quantum computation

in topologically-ordered systems where visons can be generated and displaced via local scanning techniques.

*The model*—We study numerically the Kitaev model in the presence of a uniform (perturbing) magnetic field  $\mathbf{h}$ , which allows excitations to acquire non-abelian anyonic statistics. The Hamiltonian of the system is  $\hat{H}_0 = \hat{H}_K + \hat{H}_h$ , where

$$\hat{H}_K = \sum_{\langle j,k \rangle} J_{\alpha_{jk}} \sigma_i^{\alpha_{jk}} \sigma_j^{\alpha_{jk}} \quad (1)$$

is the Kitaev Hamiltonian [20] defined on the honeycomb lattice and  $\hat{H}_h = \sum_j \mathbf{h} \cdot \boldsymbol{\sigma}_j$  is the Zeeman coupling to the external field. In these equations,  $\sigma_i^\alpha$  denotes the  $\alpha$ -th Pauli matrix acting on the spin-1/2 Hilbert space of site  $i$ . In Eq. (1),  $\langle j, k \rangle$  denotes a nearest-neighbour bond, and  $\alpha_{ij}$  takes the values  $x, y, z$  depending on the direction of the bond  $\langle j, k \rangle$  [20]. To keep the model as general as possible, the magnitude of the Ising-like coupling  $J_{\alpha_{jk}}$  is also allowed to depend on the bond direction. Hereafter, we scale energies with  $J$  (defined below) and we set  $\hbar = 1$ . Therefore, times are in units of  $J^{-1}$ .

The model can be exactly solved by mapping Pauli matrices into Majorana operators. As in [20], we introduce four Majorana operators  $b_j^x, b_j^y, b_j^z$  and  $c_j$  at each lattice site  $j$ , such that  $\sigma_j^\alpha = i b_j^\alpha c_j$ . In the Majorana representation, the Kitaev Hamiltonian becomes

$$\hat{H}_K = \sum_{jk} J_{\alpha_{jk}} b_j^{\alpha_{jk}} b_k^{\alpha_{jk}} c_j c_k. \quad (2)$$

The Majorana representation doubles the Hilbert space of the original Kitaev model [20]. The component of any state belonging to the unphysical Hilbert space is removed by operating with an opportune projector operator [20]. To define this, we introduce the gauge transformation operator  $D_j = b_j^x b_j^y b_j^z c_j$ , which satisfies  $D_j = 1$  for physical states (for which it coincides with  $-i \sigma_j^x \sigma_j^y \sigma_j^z$ ) and  $D_j = -1$  for unphysical ones [20]. The sought projector is then constructed as  $P = \prod_j (1 + D_j)/2$ , where the product is over all lattice sites  $j$ .

The Kitaev Hamiltonian in Eq. (1) possesses a set of conserved quantities  $W_p$ , which are defined for each hexagonal plaquette  $p$ . In the Majorana representation they are  $W_p = \prod_{\langle j,k \rangle} u_{jk}^{\alpha_{jk}}$ , where  $u_{jk}^{\alpha_{jk}} = i b_j^{\alpha_{jk}} b_k^{\alpha_{jk}}$ , and  $\langle j, k \rangle$  cycles through the six sides of the

hexagonal plaquette  $p$  in the counterclockwise direction. Owing to Lieb's theorem [26], the ground state of the Kitaev model must satisfy  $W_p = 1$  for any plaquette  $p$ . This state is said to be "flux free". In this paper, such state is defined by setting  $u_{ij}^{\alpha} = 1$  for  $i$  ( $j$ ) belonging to the  $A$  ( $B$ ) sublattice. When  $W_p = -1$ , the plaquette  $p$  is said to be threaded by one flux.

In the Kitaev model the spin operator  $\sigma_j^\alpha$  anti-commutes with the bond operator  $u_{jk}^\alpha$ . Therefore, applying the operator  $\sigma_j^\alpha$  to the ground state creates two vortices in the two plaquettes that share the bond  $\langle j, k \rangle$ . This suggests that one can apply a local (Zeeman) magnetic field to drive the system out of equilibrium and manipulate vortices. We therefore perturb the system with the time-dependent Hamiltonian

$$\hat{V}(t) = \sum_j \delta \mathbf{h}_j(t) \cdot \boldsymbol{\sigma}_j, \quad (3)$$

where  $\delta \mathbf{h}_j(t)$  is in the  $\hat{z}$  direction (note that its magnitude is not bound to be small with respect to  $J$ ).

*The mean-field approximation*—The magnetic field  $\mathbf{h}$  breaks the exact solvability of the model, *i.e.* the ground state of  $\hat{H}_0$  needs not to satisfy  $W_p = 1$  for all  $p$ . Thus, to determine the ground state and its time evolution under (3), we resort to a mean field decoupling of  $\hat{H}_K$ . For each bond, we decouple the four-operator term in Eq. (2) using Wick's theorem (schematically) as  $b_A^\alpha b_B^\alpha c_A c_B = \langle b_A^\alpha b_B^\alpha \rangle c_A c_B - \langle b_A^\alpha c_A \rangle b_B^\alpha c_B - \langle b_B^\alpha c_B \rangle b_A^\alpha c_A + \langle b_A^\alpha c_B \rangle b_B^\alpha c_A + \langle b_B^\alpha c_A \rangle b_A^\alpha c_B$ , where we used the sublattice indices  $A, B$  to denote the two sites of a given bond. Our treatment is similar to [27] Here,  $\alpha$  is the component of the spin that is coupled along the bond. In this way, the Hamiltonian  $\hat{H}_0$  is reduced to a quadratic form in the Majorana fermions,  $\hat{H}_{MF} = \sum H_{MF}^{ij} m_i m_j$ , where the matrix  $H_{MF}$  depends on the values of mean fields as well as on the original Hamiltonian. Hereafter, to make our notation more compact, we denote with  $\{m_j\}$  the set of all  $b_i^\gamma$  and  $c_i$  Majorana fermions (note that  $j$  here does not denote lattice sites as before).

The uniform magnetic field is taken to be  $\mathbf{h} = h \hat{\mathbf{n}}$ , where  $\mathbf{n} = (\hat{x} + \hat{y} + \hat{z})/\sqrt{3}$ . At large values of  $h$  we expect spins to polarize in the  $\hat{\mathbf{n}}$  direction, and the systems to be no longer in a spin liquid phase. In the Supplemental Information [28] we determine when this happens by solving an equilibrium mean field self-consistency equation and we calculate the spin polarization that arises from  $\mathbf{h}$ . To avoid polarizing the system, in what follows we will use small values of  $h$ .

Once equilibrium mean-fields have been determined, their time evolution is found by solving the equation of motion for  $M_{jk}(t) = \langle \psi(t) | m_j m_k | \psi(t) \rangle$ , which is  $dM/dt = 4i[H_{MF} + V(t), M]$ , where  $V_{ij}(t)$  is the matrix representation of the driving Hamiltonian:  $\hat{V}(t) = \sum_{ij} V_{ij}(t) m_i m_j$ .

In the next sections we present a protocol for generating and manipulating fluxes in the Kitaev model using the local and time-dependent Zeeman field  $\delta \mathbf{h}_j(t)$ . We consider a lattice of 64 unit cells. We employ periodic boundary conditions and we study the so-called

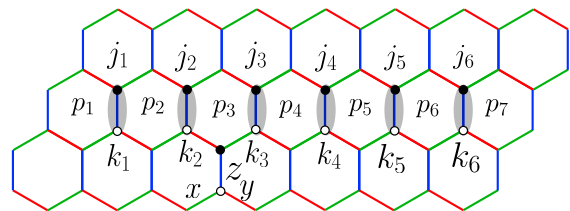


Figure 1. Illustration of the Kitaev model and of the flux manipulation protocol. The bonds of a honeycomb lattice are classified into three types, called  $x, y$  and  $z$ , colored in green, red and blue, respectively. Empty (filled) circles are sites of the  $A$  ( $B$ ) sublattice, denoted as  $j_\ell$  ( $k_\ell$ ). Sites are connected by bonds which are highlighted in dark grey. Fluxes are localised at plaquettes, which are denoted as  $p_\ell$ . At  $t = 0$ , a magnetic field in the  $z$  direction is applied simultaneously at sites  $j_1$  and  $k_1$  and turned off after time  $T$ . We repeat this procedure on the sites  $j_\ell$  and  $k_\ell$ , for  $\ell = 2, \dots, 6$ . At the end of the protocol, a pair of fluxes is created in  $p_1$  and  $p_7$ .

$A_z$  and  $B$  phases of the Kitaev model, for both ferromagnetic (FM) and antiferromagnetic (AFM) couplings. The  $A_z$  phase is gapped and it is obtained for  $|J_z| > |J_x| + |J_y|$ . In the absence of a magnetic field, the excitations of the  $A_z$  phase are abelian anyons [20]. As the gap size is of the order of  $J_z$  a small magnetic field  $h \ll J_z$  should not close it. Therefore, we conclude that the excitations in the  $A_z$  phase in the presence of a small magnetic field are still abelian anyons. The  $B$  phase is gapless and exists when  $|J_x|, |J_y|$  and  $|J_z|$  all satisfy the triangle inequality  $|J_\alpha| < |J_\beta| + |J_\gamma|$ , where  $\{\alpha, \beta, \gamma\}$  is any permutation of the three indices  $\{x, y, z\}$ . The excitations of this phase are non-abelian anyons [20]. We set  $J_x = J_y = J_z = J$  for the  $B$  phase and  $J_x = J_y = J, J_z = 2.1J$  for the  $A_z$  phase, where  $J$  can be either FM, *i.e.*  $J < 0$ , or AFM, *i.e.*  $J > 0$ .

*Flux dynamics in the FM model*—We now show flux generation and displacement in both the  $A_z$  and  $B$  phase of the FM model. We start from the  $B$  phase. We choose the uniform magnetic field to be  $h = 0.01J$  and  $|\delta \mathbf{h}_j(t)| = 0.5J$ . With reference to Fig. 1, we now show a protocol to create a pair of vortices in plaquettes  $p_1$  and  $p_7$ . We recall that the averages of bond operators on the six bonds highlighted in Fig. 1,  $u_l = u_{j_l k_l}$ , where  $l = 1, \dots, 6$ , are equal to minus one in the flux free sector, so that  $W_p$  is positive everywhere. Thus, we need to flip all six bonds  $u_1, u_2 \dots u_6$  to create the pair of vortices in the end plaquettes of the string (the only two for which  $W_p$  will be negative). The protocol we use to achieve the creation of vortices can be summarized as follows. First, we turn on a driving field  $\delta h_\ell$  with the same sign on two spin sites  $\ell = j_1$  and  $\ell = k_1$ , which results in the bond-operator average  $u_1$  to increase. We turn off the driving magnetic field after a time  $T$  for which the average of the bond operator  $u_1$  is maximal. For our parameters,  $T = 1.8J^{-1}$ . To move the flux, we then repeat the procedure on the two sites  $\ell = j_2$  and  $\ell = k_2$ , which results in the (partial) flipping of the value of  $u_2$ . Repeating the process for all other bonds, we eventually create a flux pair at  $p_1$  and  $p_7$ .

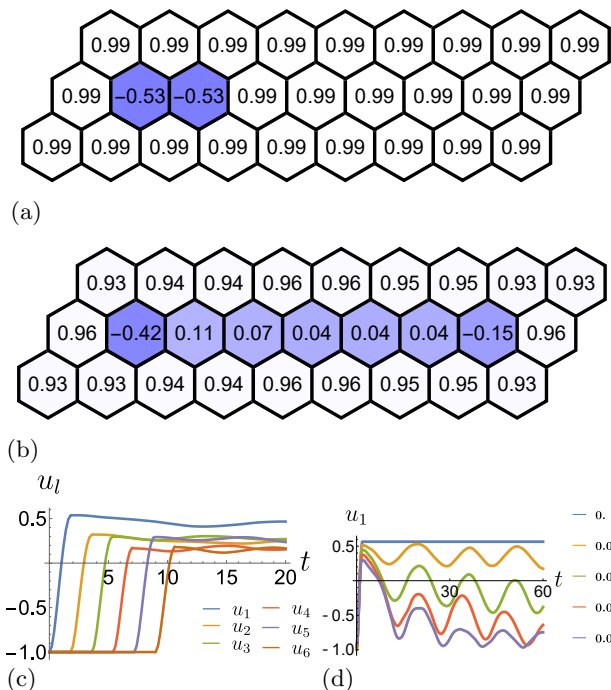


Figure 2. Flux manipulation protocol applied to the  $B$  phase of the FM model. Panel (a) the flux configuration at time  $t = T$ . The magnetic field applied on the bond  $B_1$  (see Fig. 1) has partially flipped the fluxes in plaquettes  $p_1$  and  $p_2$ . Panel (b) The flux configuration at the end of the protocol ( $t = 20J^{-1}$ ). Panel (c) The time evolution of the bond variables  $u_l$ . Panel (d) The time evolution of  $u_1$  for different values of the uniform field  $h$ . The driving field was applied at sites  $k_1$  and  $j_1$ , and turned off at the time when each curve reaches its maximum.

The results of this protocol are shown in Figs. 2(a)-(b). In Fig. 2(a) we show that applying the driving fields  $\delta h_{j_1}$  and  $\delta h_{k_1}$  for a time  $T$  has flipped the value of  $u_1$ , although not completely. For the parameters stated above, we reach  $u_1 \approx 0.5$ , which corresponds to  $W_{p_1} = W_{p_2} = -0.5$ . This corresponds to generating a state which, in each plaquette  $p$ , is in a superposition between a vortex and no-vortex state, with probability  $(1 - W_p)/2 \approx 0.75$  to have a pair of vortices, and probability  $(1 + W_p)/2 \approx 0.25$  to have no vortex.

Repeating this procedure for all other bonds in the string, we see that we can only achieve  $u_l \approx 0.2$  for  $l = 2, \dots$ . Thus, for intermediate plaquettes the probability of having a vortex is very close to one half. The value of the flux operator is relatively large and negative in the first and last plaquettes. This corresponds to a probability of having a flux equal to  $\approx 0.7$  and  $\approx 0.58$  in the first and last plaquettes, respectively. The vortices we create are quite stable, as shown by the flat time evolution of the  $u_l$ 's shown in Fig. 2(c).

We now study the stability of a flux pair as a function of the uniform field  $h$ . We apply a local driving field  $\delta h_\ell = 0.5J$  only at the sites  $\ell = j_1$  and  $\ell = k_1$ , and we turn it off when the maximum value of  $u_1$  has been reached. We show the evolution of  $u_1$  for subsequent times in Fig 2(d). In the absence of the field  $h$ , the fluxes are protected by the  $Z_2$  symmetry of the unperturbed Kitaev model, as evidenced by the straight line in Fig. 2(d). For finite  $h$ , we find that  $u_1$  oscillates

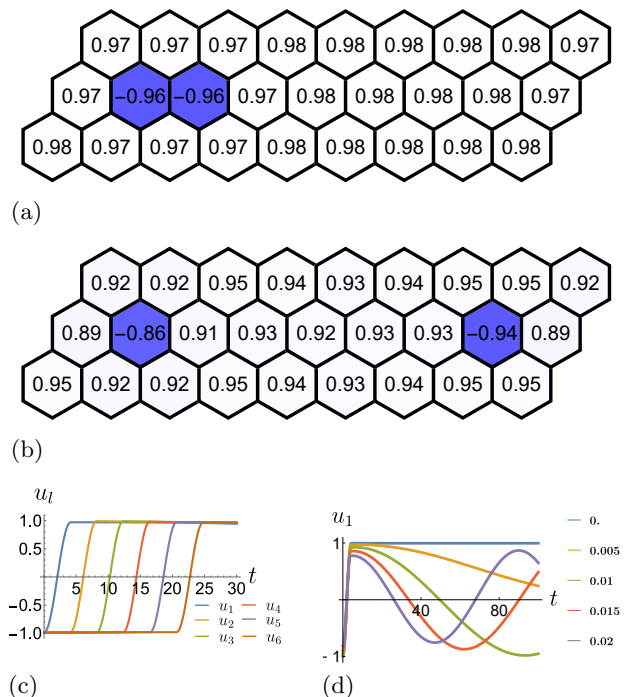


Figure 3. Flux manipulation protocol applied to the  $A_z$  phase of the FM model. Panel (a) the flux configuration at time  $t = T$ . The magnetic field applied on the bond  $B_1$  (see Fig. 1) has nearly-completely flipped the fluxes in plaquettes  $p_1$  and  $p_2$ . Panel (b) The flux configuration at the end of the protocol ( $t = 30J^{-1}$ ). Panel (c) The time evolution of the bond variables  $u_l$ . Panel (d) The time evolution of  $u_1$  for different values of the uniform field  $h$ . The driving field was applied at sites  $k_1$  and  $j_1$ , and turned off at the time when each curve reaches its maximum.

lates with an amplitude that increases with  $h$ . For  $h = 0.02J$ , the oscillation appears to be sinusoidal. At larger  $h$ , such as  $h = 0.04J$ , the flux pair appears to be unstable.

In the Supplemental Information [28] we also show that the maximum value reached by the bond variable  $u_1$  becomes smaller for large values of  $h$ . Though the uniform field is needed to obtain non-abelian anyonic excitations, our results show that  $h$  should be kept as small as possible for fluxes to be generated with high probability and to remain stable.

We then apply the same protocol to create a pair of fluxes in the  $A_z$  phase of the FM model. In this case, we use the parameters  $T = 4.1J^{-1}$ ,  $h = 0.005J$  and  $\delta h = 0.2J$ . The results are shown in Figs. 3(a)-(b). In Fig. 3(a) we show that, starting from the uniform flux-free configuration and applying the driving fields  $\delta h_{j_1}$  and  $\delta h_{k_1}$  for a time  $T$ , the value of  $u_1$  is almost completely flipped. For the parameters used, we can reach  $u_1 \approx 0.97$ , which corresponds to generating fluxes in  $p_1$  and  $p_2$  with probability  $\approx 1$ . Repeating this procedure for all other bonds in the string, we see that we can achieve  $u_l \approx 1$  for  $l = 2, \dots$ . Thus, the intermediate plaquettes remain almost flux free in this case, and fluxes are almost completely localised at the end plaquettes of the string. The probability of having a flux is equal to  $\approx 0.93$  and  $\approx 0.97$  for the first and last plaquettes, respectively. The vortices we create

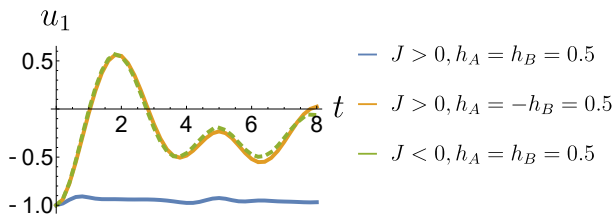


Figure 4. The time evolution of  $u_1$  under a constant driving field  $|\delta h_\ell| = 0.5J$ . The FM case with  $\delta h_A = \delta h_B$  is almost identical to the AFM case with  $\delta h_A = -\delta h_B$ .

are very stable, as shown by the flat time evolution of the  $u_i$ 's shown in Fig. 3(c). Clearly, our protocol works much better in the  $A_z$  phase than the  $B$  phase.

Next, we analyse the stability of the flux pair in the  $A_z$  phase. As before, we apply a local driving field  $\delta h_\ell = 0.2J$  only at sites  $\ell = j_1$  and  $\ell = k_1$ , and we study the time evolution of  $u_1$ . In Fig 3(d) we present the time evolution of  $u_1$  for different values of  $h$  after turning off the local driving field  $\delta h$  when the maximum value has been reached. In the absence of the field  $h$ , the fluxes are again protected by the  $Z_2$  symmetry of the unperturbed Kitaev model. On the other hand, for finite  $h$ , we find that the bond  $u_1$  oscillates with a frequency that increases with larger  $h$ . The oscillations appear to be sinusoidal for all  $h$ , with amplitudes largely independent of  $h$ . In the  $h = 0.005J$  case, judging from the pattern it is likely that it will also reach  $-1$  after a much longer time than what afforded by our simulations.

*Flux dynamics in the AFM model*—In the AFM model, we find that the above protocol needs modification. We focus on the  $B$  phase, as modifications are similar for the  $A_z$  phase. As shown in Fig 4, if the field  $\delta h_\ell$  takes the same value on both sites  $\ell = j_1$  and  $\ell = k_1$  (which belong to different sublattices), the value of the bond operator  $u_1$  remains very close to  $-1$ . Thus, no flux will be created. However, if the driving magnetic field takes opposite signs on the two sublattices, then we find that the time evolution of  $u_1$  is almost identical to that of the ferromagnetic model. This is not by chance, and it is due to a symmetry in the model that allows us to translate almost perfectly the results found for the FM model to the AFM one.

To understand this behaviour, we define the operator  $O_A = \prod_{j \in A} \theta_j$ , where  $\theta_j \equiv b_j^x b_j^y b_j^z$ , and the product is taken over the  $A$  sublattice sites only. Note that, because the  $\theta_j$ 's anti-commute with each other, the order of the terms in the product must be kept fixed throughout the calculation. The operator  $O_A$  anti-commutes with the spins in  $A$  sublattice, but commutes with the  $B$  sublattice spins. Since  $O_A$  is unitary, we can use it to transform every observable  $\hat{X}$  as  $\hat{X} \rightarrow O_A^\dagger \hat{X} O_A$ , and every state  $|\psi\rangle$  as  $|\psi\rangle \rightarrow O_A^\dagger |\psi\rangle$ . In particular, the Hamiltonian transforms as

$$O_A^\dagger \hat{H}_K O_A = -\hat{H}_K, \quad (4)$$

therefore  $O_A$  turns a ferromagnetic Kitaev model into an antiferromagnetic one, and vice versa. The driving

Hamiltonian (3) gets transformed into

$$O_A^\dagger V O_A = \sum_i (-\delta h_{i,A} \sigma_{i,A} + \delta h_{i,B} \sigma_{i,B}), \quad (5)$$

where  $i$  here denotes the unit cell to which the spins of the two sublattices belong. Therefore, the operator  $O_A$  reverses the sign of the magnetic field  $h_{i,A}$  applied on  $A$  sublattice sites, while keeping the field on  $B$  sublattice sites unchanged.

Thus the FM model with a small uniform magnetic field  $h$  and a driving field  $\delta h = \delta h_A = \delta h_B$  that has the same sign on the two sublattices (as in Fig 4) is mapped into the AFM one with staggered  $h$  and  $\delta h$ . This fact indicates that our results for the FM model can be carried over to the AFM one with little modifications, as shown in Fig. 4. The small discrepancy between the FM and the AFM model with  $\delta h_A = -\delta h_B$ , is due to the fact that the sign of the uniform field  $h$  has been kept the same on both sublattices.

*Conclusions*—We have numerically studied the Kitaev model in the presence of uniform and local driving magnetic fields with a combination of mean-field and exact-diagonalization techniques. We have studied the effect of a time-dependent and local driving magnetic field with a dynamical mean-field approach (where the dynamics of mean-fields is generated by the applied magnetic field). We have demonstrated that such magnetic field can be used to create and move vortices in both the FM and AFM Kitaev model. We found the optimal parameters for such processes, and discussed the stability and quality of the fluxes produced. We also show that there is a one-to-one correspondence between the FM and AFM Kitaev models.

Our protocol for vortex creation and manipulation relies on a magnetic field that is applied to a very small region of space. It may be slightly challenging to achieve such localisation in real experiments. We do not discuss this issue here, as the focus of this work is on the capability of generating *in principle* flux pairs with local fields. While this is a limitation of our work, which will be analysed in more detail in the future, we wish to stress that our work may be applicable to quantum phases emerging in, e.g., twisted systems. In these systems, the typical scales of spin localisation are much larger and allow one to relax the requirement of extreme locality of the applied field.

While this manuscript was being prepared a related work [29] was made public on arXiv. There, the dynamics of the “extended Kitaev model” in the presence of local magnetic fields was studied. The model of Ref. [29] approximates the effect of the uniform magnetic field in the perturbative regime  $|h| \ll |J|$  with a three-spin term. The latter gives rise to a Haldane-type next-nearest-neighbour hopping term for the  $c$ -Majorana fermions [20]. Thus, it is responsible for opening a gap in the  $B$  phase and for the emergence of edge Majorana particles.

There are significant differences between the dynamics of our model, and the one studied in Ref. [29] which can be traced back to the approximate nature



of the latter. In the model of Ref. [29] a threshold behaviour is found whereby fluxes can be created with probability one if the local magnetic field is above a certain value. In our model, which treats the uniform field in a non-perturbative way, we find that we can at best generate a flux with probability of  $\approx 0.75$ . Furthermore, in our model the uniform field  $\mathbf{h}$  breaks the conservation of fluxes, and we showed that fluxes are actually highly unstable at large enough fields. In the model of Ref. [29], however, fluxes are conserved by construction. Additionally, their choice of uniform magnetic field ( $\kappa = 0.05J$ ) corresponds to a magnetic field for which the spin polarization is very large ( $\approx 0.8$ , see [28]). This questions the validity of the extended model as a good approximation of the Kitaev model in a uniform magnetic field. Such model in fact relies on perturbatively building an effective Hamiltonian in the flux free sector, where the spin polarization is zero.

*Acknowledgments*—We acknowledge support from the European Commission under the EU Horizon 2020 MSCA-RISE-2019 programme (project 873028 HYDROTRONICS) and from the Leverhulme Trust under the grant agreement RPG-2019-363.

---

\* [haoran.wang-6@postgrad.manchester.ac.uk](mailto:haoran.wang-6@postgrad.manchester.ac.uk)

† [alessandro.principi@manchester.ac.uk](mailto:alessandro.principi@manchester.ac.uk)

- [1] I. L. Chuang, R. Laflamme, P. W. Shor, and W. H. Zurek, *Science* **270**, 1633 (1995).
- [2] W. H. Zurek, *Reviews of modern physics* **75**, 715 (2003).
- [3] K. Hornberger, *Entanglement and Decoherence: Foundations and Modern Trends*, 221 (2009).
- [4] M. A. Schlosshauer, *Decoherence: and the quantum-to-classical transition* (Springer Science & Business Media, 2007).
- [5] W. H. Zurek *et al.*, *Physics today* **44**, 36 (1991).
- [6] P. W. Shor, *Physical review A* **52**, R2493 (1995).
- [7] S. P. Jordan, E. Farhi, and P. W. Shor, *Physical Review A* **74**, 052322 (2006).
- [8] E. Knill and R. Laflamme, *Physical Review A* **55**, 900 (1997).
- [9] P. W. Shor, in *Proceedings of 37th conference on foundations of computer science* (IEEE, 1996) pp. 56–65.
- [10] D. G. Cory, M. Price, W. Maas, E. Knill, R. Laflamme, W. H. Zurek, T. F. Havel, and S. S. Somaroo, *Physical Review Letters* **81**, 2152 (1998).
- [11] J. Chiaverini, D. Leibfried, T. Schaetz, M. D. Barrett, R. Blakestad, J. Britton, W. M. Itano, J. D. Jost, E. Knill, C. Langer, *et al.*, *Nature* **432**, 602 (2004).
- [12] E. Knill, R. Laflamme, R. Martinez, and C. Negrevergne, *Physical Review Letters* **86**, 5811 (2001).
- [13] M. Freedman, A. Kitaev, M. Larsen, and Z. Wang, *Bulletin of the American Mathematical Society* **40**, 31 (2003).
- [14] A. Kitaev, *Annals of Physics* **303**, 2 (2003).
- [15] E. Dennis, A. Kitaev, A. Landahl, and J. Preskill, *Journal of Mathematical Physics* **43**, 4452 (2002).
- [16] A. Stern and N. H. Lindner, *Science* **339**, 1179 (2013).
- [17] S. Das Sarma, M. Freedman, and C. Nayak, *Physics today* **59**, 32 (2006).
- [18] X. G. Wen and Q. Niu, *Phys. Rev. B* **41**, 9377 (1990).
- [19] C. Nayak, S. H. Simon, A. Stern, M. Freedman, and S. D. Sarma, *Reviews of Modern Physics* **80**, 1083 (2008).
- [20] A. Kitaev, *Annals of Physics* **321**, 2 (2006).
- [21] M. Hermanns, I. Kimchi, and J. Knolle, *Annual Review of Condensed Matter Physics* **9**, 17 (2018).
- [22] G. Jackeli and G. Khaliullin, *Physical review letters* **102**, 017205 (2009).
- [23] H. Takagi, T. Takayama, G. Jackeli, G. Khaliullin, and S. E. Nagler, *Nature Reviews Physics* **1**, 264 (2019).
- [24] S. M. Winter, A. A. Tsirlin, M. Daghofer, J. van den Brink, Y. Singh, P. Gegenwart, and R. Valentí, *Journal of Physics: Condensed Matter* **29**, 493002 (2017).
- [25] M. Gohlke, R. Moessner, and F. Pollmann, *Physical Review B* **98**, 014418 (2018).
- [26] E. H. Lieb, *Physical Review Letters* **73**, 2158 (1994).
- [27] T. Minakawa, Y. Murakami, A. Koga, and J. Nasu, *Physical review letters* **125**, 047204 (2020).
- [28] See the Supplemental Information online.
- [29] C. Harada, A. Ono, and J. Nasu, *arXiv preprint arXiv:2305.08357* (2023).
- [30] H.-C. Jiang, Z.-C. Gu, X.-L. Qi, and S. Trebst, *Physical Review B* **83**, 245104 (2011).

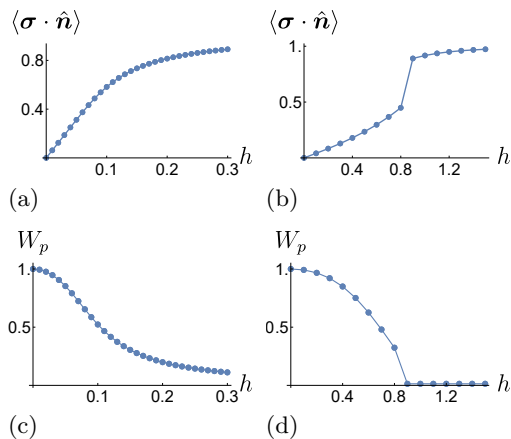


Figure 5. Panel (a) The spin polarization of the  $B$  phase along the direction of the external magnetic fields in the FM model. Panel (b) Same as Panel (a) but for the AFM model. A clear phase transition occurs at  $h \approx 0.85$ . Panel (c) The average of the flux operator  $\langle W_p \rangle$  as a function of the magnetic field  $h$  for  $B$  phase of the FM model. Panel (d) Same as Panel (c) but for the AFM model. In both cases  $\langle W_p \rangle$  is independent of  $p$  because of the periodicity of the system.

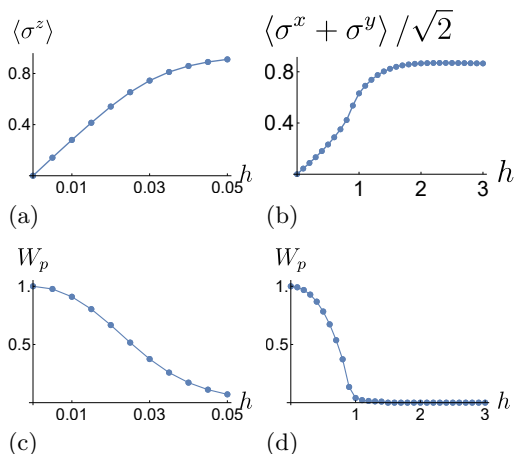


Figure 6. Panel (a) The spin polarization of the  $A_z$  phase along the direction of the external magnetic fields in the FM model. Panel (b) Same as Panel (a) but for the AFM model. A phase transition occurs at  $h \approx 1J$ . Panel (c) The average of the flux operator  $\langle W_p \rangle$  as a function of the magnetic field  $h$  for  $A_z$  phase of the FM model. Panel (d) Same as Panel (c) but for the AFM model. In both cases  $\langle W_p \rangle$  is independent of  $p$  because of the periodicity of the system.

### Spin polarization

To find the ground state of the Hamiltonian  $H_0$  treated within the mean-field approximation, we derive and solve static mean-field self-consistent equations as follows. Firstly, we assume an initial value for  $\langle m_i m_j \rangle$  and diagonalize the Hamiltonian  $\hat{H}_{MF}$ . We obtain  $\hat{H}_{MF} = \sum_k \epsilon_k a_k^\dagger a_k$ , where  $k$  labels the eigenmodes of the system and the  $m_i$ 's are related to the  $a_k$ 's according to  $m_i = S_{ik} a_k$ . Here,  $S_{ik}$  is a unitary matrix. Since we are looking for the lowest energy state, the average  $\langle a_k^\dagger a_k \rangle$  is equal to one

whenever  $\epsilon_k < 0$ , and zero otherwise. It follows that  $\langle m_i m_j \rangle = \sum_{\epsilon_k < 0} S_{ik}^* S_{jk}$ . This gives us a new Ansatz for the mean fields, which we plug back into  $\hat{H}_{MF}$ . We repeat the process until convergence. We stop the iterations when the sum of the absolute values of the differences between the averages for two consecutive steps is below  $10^{-6}$ .

The spin polarization along the direction of the magnetic field,  $\langle \sigma \cdot \hat{n} \rangle$ , for the  $B$  phase of the FM [AFM] model is shown in Fig. 5(a) [(b)]. In Figs. 5(c) and (d) we show instead the average value of the flux operator  $W_p$  of the FM and AFM models, respectively. In both cases,  $W_p$  is expected to approach zero, since it becomes equally likely to have one or no vortex in any plaquette at high magnetic fields. Similarly, Fig. 6(a) [(b)] shows  $\langle \sigma \cdot \hat{n} \rangle$  for the  $A_z$  phase of the FM [AFM] model, while Fig. 6(c) [(d)] shows the average value of  $W_p$  of the FM [AFM] model.

In the FM model, for both the  $B$  and the  $A_z$  phases, we find that the polarization rises smoothly, approaching one only in the limit of infinite field. In both cases we do not find a clear phase transition point. However, the polarization is in the  $\hat{n}$  direction for the  $B$  phase, while for  $A_z$  phase it is mostly in the  $z$  direction, with the component in the  $x, y$  plane much smaller than  $\langle \sigma^z \rangle$ . Furthermore, the polarization  $\langle \sigma^z \rangle$  rises much faster in the  $A_z$  phase, which approaches 0.8 at around  $h \approx 0.03J$ , while in the  $B$  phase it takes  $h \approx 0.2J$  to achieve  $\langle \sigma \cdot \hat{n} \rangle \approx 0.8$ . The result for the  $B$  phase is at odds with Ref. [30], which finds a singularity in the first derivative of the magnetization at around  $h \approx 0.085J$  using density-matrix renormalization group methods. We attribute this to limitations of the mean-field approach. However, in agreement with Ref. [30], we find that in both cases  $W_p$  vanishes smoothly. Both curves, in Fig. 5(c) and in Ref. [30], show an initially flat region where  $W_p$  does not change much, followed by a steep descent, to then smoothly converge to zero in the limit of infinite  $h$ . These contrasting results show that, though the mean-field approximation has limitation in describing certain features of thermodynamic quantities, it is capable of capturing the general behaviour of vortices. This lends credibility to the studies of the main text.

Contrary to the previous cases, in the AFM model, we find a clear sign of phase transition in both  $B$  and  $A_z$  phases. In the  $B$  phase, at  $h \approx 0.85J$ , the spin polarization jumps discontinuously, as shown in Fig. 5(b). At the same critical field, the average flux  $W_p$  vanishes exactly, and remains equal to zero for higher fields, as shown in Fig. 5(d). In the  $A_z$  phase, the jump in polarization which occurs at  $h \approx 1J$ , is less clear, as shown in Fig 6(b). The same critical point is easier to identify in Fig. 6(d), which shows that the average flux  $W_p$  clearly vanishes at  $h \approx 1J$  and remains zero for higher fields.

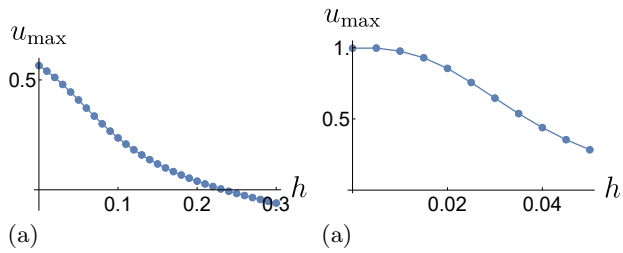


Figure 7. The maximum value attained by  $u_1$  under a quench of the local magnetic field  $\delta h$  applied at the spin sites  $k_1$  and  $j_1$  (see Fig. 1 in main text), for different values of  $h$ . Panel (a) The  $B$  phase of the FM model. Panel (b) The  $A_z$  phase of the FM model.

### Optimal value of the magnetic field

Here we investigate the optimal value of the uniform field  $h$  to achieve flux creation. In the  $B$  phase, we apply a local driving field  $\delta h_\ell = 0.5J$  only at sites  $\ell = j_1$  and  $\ell = k_1$ , and we study the time evolution for different values of the uniform field  $h$ . From this, we calculate the maximum value reached by the bond operator  $u_1$  over time (given the applied uniform field  $h$ ). We find that  $u_{\max}$  is maximum at  $h = 0$ , as shown in Fig. 7(a). This is further proof that it is best to keep the uniform magnetic field as small as possible.

In the  $A_z$  phase, we apply a local driving field  $\delta h_\ell = 0.2J$  only at sites  $\ell = j_1$  and  $\ell = k_1$ . Using the same procedure used for the  $B$  phase, we find that  $u_{\max}$  steadily decreases with  $h$ , as shown in Fig. 7(b). Thus, the optimal value of the magnetic field is zero in this case.